J Solid State Electrochem (2018) 22:705–715
https://doi.org/10.1007/s10008-017-3796-8

ORIGINAL PAPER

# Direct fabrication of anatase $TiO_2$ hollow microspheres for applications in photocatalytic hydrogen evolution and lithium storage

**Shuai Shi**[1] · **Yang Chen**[1] · **Jordan Lee**[1] · **Zhiyu Jiang**[2] · **Xiaoli Cui**[1]

Received: 18 April 2017 / Revised: 30 September 2017 / Accepted: 4 October 2017 / Published online: 18 October 2017


**Abstract** Hollow titanium dioxide ($TiO_2$) microspheres were synthesized in one step by employing tetrabutyl orthotitanate (TBOT) as a precursor through a facile solvothermal method in the presence of $NH_4HCO_3$. XRD analysis indicated that anatase $TiO_2$ can be obtained directly without further annealing. $TiO_2$ hollow microspheres with diameters in the range of 1.0–4.0 μm were confirmed through SEM and TEM measurements. The specific surface area was measured to be 180 $m^2\ g^{-1}$ according to the nitrogen adsorption–desorption isotherms. Superior photocatalytic performance and good lithium storage properties were achieved for resultant $TiO_2$ samples. The $H_2$ evolution rate of the optimal sample is about 0.66 mmol $h^{-1}$ after loaded with 1 wt.% Pt (20 mg samples). The reversible capacity remained 143 mAh $g^{-1}$ at a specific current of 300 mA $g^{-1}$ after 100 charge–discharge cycles. This work provides a facile strategy for the preparation of hollow titanium dioxide microspheres and demonstrates their promising photocatalytic $H_2$ evolution and the lithium storage properties.

**Keywords** $TiO_2$ hollow microspheres · Energy conversion · Lithium-ion battery · Photocatalysis · Hydrogen evolution

**Electronic supplementary material** The online version of this article (https://doi.org/10.1007/s10008-017-3796-8) contains supplementary material, which is available to authorized users.

✉ Xiaoli Cui
xiaolicui@fudan.edu.cn

[1] Department of Materials Science, Fudan University, Shanghai 200433, China

[2] Department of Chemistry, Fudan University, Shanghai 200433, China

## Introduction

$TiO_2$ has been extensively considered as a potential anode candidate in rechargeable batteries and an efficient photocatalyst for water splitting, dye-sensitized solar cells and degradation of organic pollutants, in order to deal with the urgent issues of energy storage and conversion, as well as environmental crisis [1–4]. $TiO_2$ is multifunctional material with the inherent advantages of low cost, non-toxicity, good chemical stability and environmental benignity. It has drawn great interests on photocatalytic hydrogen evolution due to its better carrier mobility, good electron-hole separation ability, higher conduction band edge energy and higher redox driving force [1, 5, 6]. Several micro-/nanostructured $TiO_2$ such as nanotubes [7], nanobelts [8], nanosheets [9] and hollow microspheres [10, 11] have been used for $H_2$ evolution.

$TiO_2$ has also been studied as a promising anode material for lithium-ion batteries (LIBs) because of its high energy density, long cycling life and small volume expansion (< 4%) during $Li^+$ insertion–extraction process [12–24]. However, there are still some intrinsic drawbacks of $TiO_2$ such as poor electronic conductivity and low ionic diffusion efficiency, which limit its further application for lithium storage. To overcome above issues, various forms of structure including nanostructure [12], hierarchical structure [18], mesoporous structure [19] have been designed in order to enlarge the contact area between electrolyte and solid electrodes and shorten the transfer pathway of lithium ions [3, 4, 20, 21].

Combining the inherent defects and potential utilization of $TiO_2$ both as a promising photocatalytic reagent and an alternative anode material for lithium ion batteries, it is essential to fabricate $TiO_2$ with large specific surface area, high crystallinity, enhanced light adsorption and rapid lithium ions transfer channels [25–27].

It has been realized that hollow structure can enhance light absorption and the rapid transport of lithium ions [28–30]. While microspherical morphology has been reported to be beneficial to multiple reflections of the incident light, resulting in high photon absorption associated with light scattering [31, 32]. $TiO_2$ hollow microspheres have attracted much attention due to the large specific surface area [33, 34].

Many strategies have been proposed to synthesize $TiO_2$ hollow microspheres [35–43]. The hard-template method that employs silica spheres [37], carbon spheres [39], polystyrene beads [40], or other spherical particles as removable templates has been considered to be the most direct and effective way to fabricate $TiO_2$ hollow microspheres. Recently, Liu et al. [37] prepared $TiO_2$ hollow microspheres by sintering $SiO_2$-$TiO_2$ core–shell structural spheres at 500 °C for 5 h and then etching with 5% HF to remove $SiO_2$. Wang et al. [38] synthesized $TiO_2$ hollow microspheres through a sol-gel process by using carbon spheres as templates. Zhong et al. [40] obtained $TiO_2$ hollow microspheres by templating the precursor solutions against crystalline arrays of monodisperse polystyrene beads. Although the hard-template method is a universal and straightforward method, some problems with this method remain, such as complex process, toxic reagent, residual impurity, time consuming or high cost.

In this work, we report a simple template-free method to synthesize anatase $TiO_2$ hollow microspheres in one step. As expected, the resultant sample shows a superior rate performance in lithium-ion batteries, great adsorption ability of organic pollutants and excellent photocatalytic water splitting performance for $H_2$ evolution.

## Experimental

### Synthesis of $TiO_2$ hollow microspheres

Tetrabutyl titanate (chemically pure), anhydrous ethanol (guaranteed reagent) and $NH_4HCO_3$ (analytical reagent) were purchased from Sinopharm Chemical Reagent Co., Ltd. (China). All chemicals were used without further purification. In a typical experiment, 1 mL TBOT and 7 mL anhydrous ethanol were dropped into a 25-mL beaker, followed by ultrasonication and constantly stirring. Then, 4 g $NH_4HCO_3$ was added into a 100-mL Teflon-lined autoclave. Subsequently, the beaker with mixed solution was transferred into the autoclave, as shown in Scheme 1. The autoclave was maintained at 250 °C for 3, 6, and 10 h. After cooling down to room temperature, the products were obtained by rinsing with deionized water and then drying at 60 °C overnight.

### Characterizations

The morphology and microstructure of the samples were characterized using a scanning electron microscope (Philips, XL30FEG) and a transmission electron microscope (TECNAI, G2F20). The crystal structure of the samples was analyzed using an X-ray diffractometer (Bruker, D/8). The nitrogen adsorption-desorption isotherms were performed using a surface area and pore size analyzer (Quantachrome, Quadrasorb evo) at 77 K, the specific surface area of the samples was calculated according to the Brunauer–Emmett–Teller (BET) equation. UV-vis diffuse reflectance spectra were obtained with a UV-vis spectrophotometer (Shimadzu, UV 3600) using barium sulfate powder as a standard.

### Adsorption property for MB

Adsorption test for methylene blue (MB) was carried out to evaluate the adsorption performance of the as-prepared samples. Typically, 50 mg sample was introduced into 50 mL MB solution (20 mg $L^{-1}$) in a quartz container. The mixed suspension was stirred for 5 h at room temperature in dark to reach the adsorption equilibrium status. Then, the powders were removed by centrifugation, and the residual MB solution was determined by its absorption spectrum at 664 nm, which

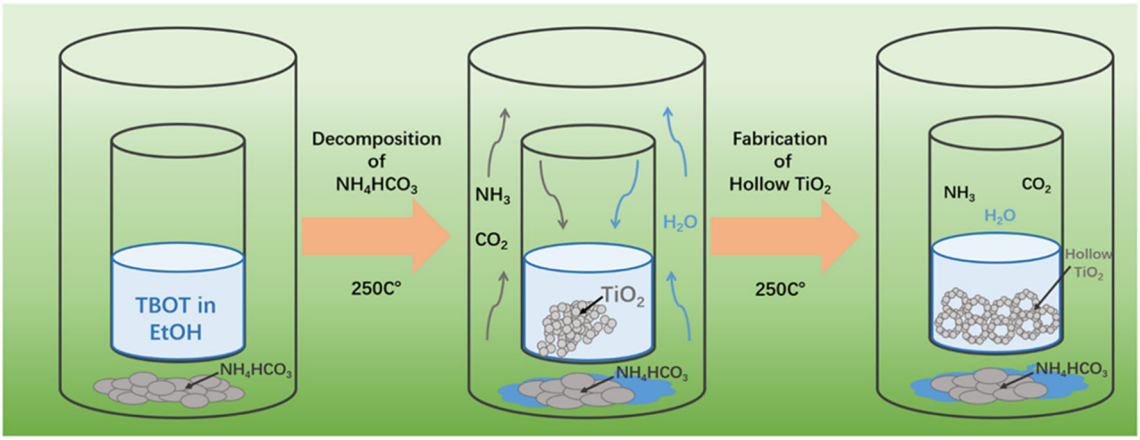


**Scheme 1** Schematic illustration of the preparation process for $TiO_2$ hollow spheres

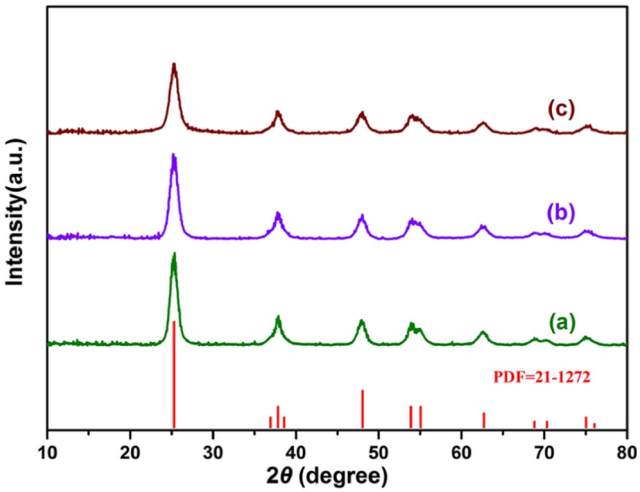


**Fig. 1** XRD patterns of the hollow $TiO_2$ samples prepared for 3 h (a), 6 h (b), and 10 h (c)

was recorded on a UV-2300 spectrophotometer. Thus, the equilibrium adsorption amount of MB was calculated according to Eq. (1) [42].

$$Q_e = (C_0 - C_e) \cdot V/m \quad (1)$$

where $Q_e$ (mg $g^{-1}$) is the equilibrium adsorption amount of MB, $C_0$ and $C_e$ (mg $L^{-1}$) is the initial and equilibrium centration of MB, respectively. $V$ (L) is the volume of MB solution, and $m$ (g) is sample mass.

## Photocatalytic hydrogen generation

1 wt.% platinum nanoparticles were loaded onto the hollow $TiO_2$ samples as a kind of co-catalyst to facilitate photocatalytic hydrogen production by a photo-deposition method. In a typical experiment, 100 mg hollow $TiO_2$ powders, 2 mL methanol, 50 mL deionized water and a certain amount $H_2PtCl_6 \cdot 6H_2O$ were mixed to form a homogeneous suspension. The

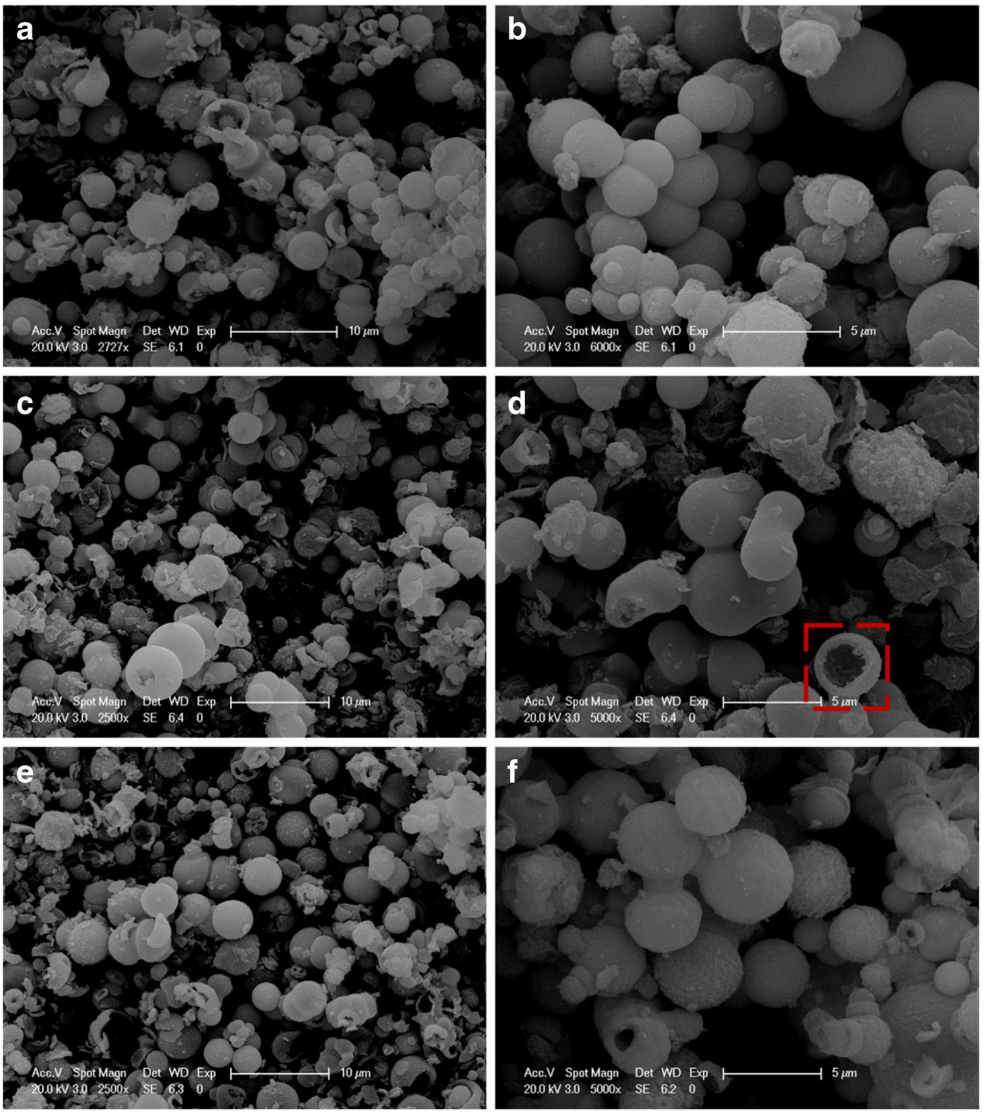


**Fig. 2** SEM images of the hollow $TiO_2$ samples prepared for **a**, **b** 3 h; **c**, **d** 6 h; and **e**, **f** 10 h

mixed solutions were irradiated by a mercury light source for 30 min at room temperature and then stirred 1 h under dark condition. The Pt loaded samples were gained after centrifugation and drying. The photocatalytic hydrogen generation tests were performed in a top-irradiation reactor connected to a gas-insulated circulation and evacuation system (Perfect Light Labsolar-III AG). Typically, 20 mg Pt loaded sample powders and 10 mL methanol were dispersed into 90 mL deionized water, which was then sealed and evacuated in the reactor. Before reaction, the whole system was pumped out to remove the air. The reaction solution was irradiated under stirring condition by using a 300 W Xe arc lamp (Perfect Light, PLS-SXE300, 300–2000 nm) as an external light source. The lamp was placed 4 cm away from the reaction vessel. The gas component was analyzed using an online gas chromatograph (Shiweipx, GC7806) equipped with a thermal conductivity detector (TCD) and molecular sieve (5 Å pore size). High purity nitrogen was used as the carrier gas.

### Electrochemical measurements

The electrochemical properties of the $TiO_2$ samples were also investigated as anode materials in CR2016-type coin cells. Prior to use, the as-prepared samples were dried at 100 °C under vacuum for 24 h to remove surface adsorbed water. The working electrode was composed of active component ($TiO_2$ hollow microspheres), conductive agent (Super P) and polymer binder (polyvinylidene fluoride, PVDF), a mixture of these three components in a weight ratio of 8:1:1 was stirred and dispersed in N-methyl-2-pyrrolidone (NMP) solvent and then evenly pasted on a copper foil, followed by drying at 60 °C for 24 h under vacuum. Metal lithium was employed as the counter electrode, and a polymer film (Celgard-2300) served as the separator. The electrolyte was 1.0 M $LiPF_6$ dissolved into a mixture of ethylene carbonate (EC) and dimethyl carbonate (DMC) (1:1 in volume). The cells were assembled in Ar-filled glove box with a concentration of moisture and oxygen below 1.0 ppm. Cyclic voltammetry (CV) was recorded using an electrochemical workstation (CHI 601D, CH Instruments) at a scan rate of 0.2 mV $s^{-1}$. Galvanostatic charge–discharge cycling was conducted on CT2001A battery tester system (Wuhan LAND Electronic Co., Ltd). Electrochemical impedance spectroscopy (EIS) was collected on PARSTAT 4000 (Princeton Applied Research) over a frequency range from 100 kHz to 0.01 Hz with a 5-mV amplitude. Both cells were discharged-charged for 30 cycles before EIS measurement in order to reach the stable states.

## Results and discussion

Figure 1 illustrates XRD patterns of the $TiO_2$ samples prepared for different solvothermal reaction time. All observed diffraction peaks of each sample can be well-indexed to the anatase phase of $TiO_2$ according to JCPDS card No. 21-1272 [44]. The sharp peaks indicate that pure anatase $TiO_2$ with high crystallization can be directly obtained after 3 h. No detectable effect on the formation of anatase phase was observed with extending of reaction time to 10 h. According to the full width at half maximum of (101) lattice plane, the grain size of each sample was approximately 10 nm based on the Scherrer equation [12].

Figure 2 displays SEM images of the samples prepared for 3 h (a, b), 6 h (c, d), and 10 h (e, f). The $TiO_2$ microspheres

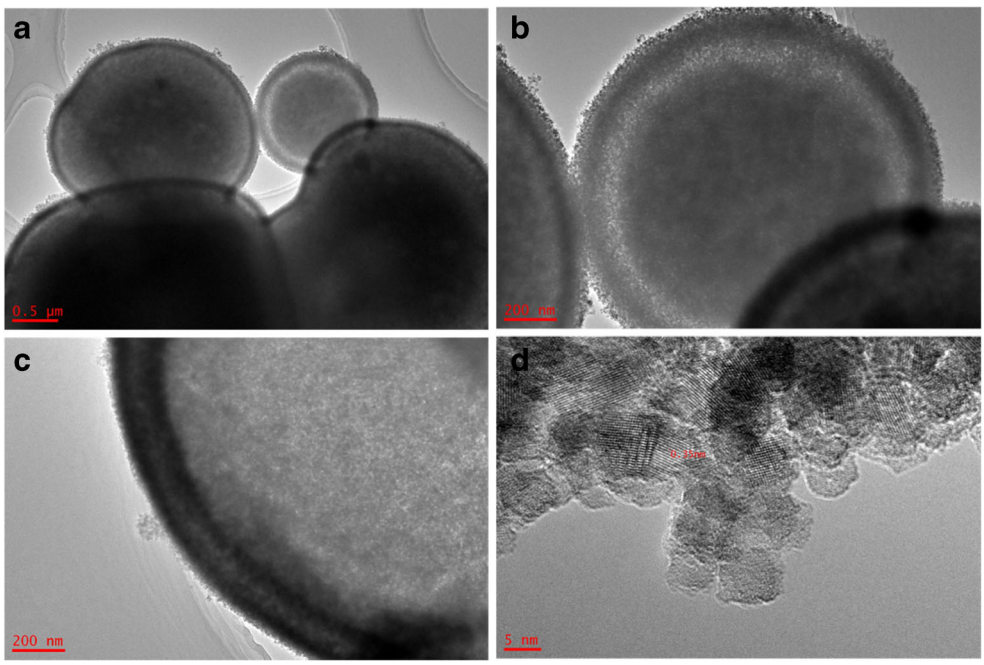


**Fig. 3** **a-c** TEM images of the hollow $TiO_2$ sample prepared for 10 h at different magnification; **d** High-resolution TEM image of the hollow $TiO_2$ sample

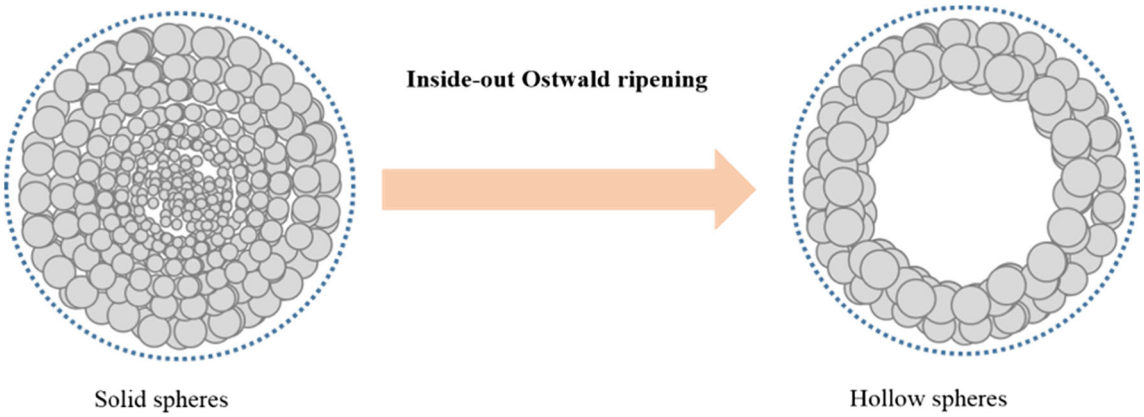


**Scheme 2** Schematic illustration of the formation mechanism of $TiO_2$ hollow spheres

with diameters in the range of 1.0–4.0 μm can be obtained after solvothermal process of 3 h, and no enlargement of particle size can be found even the reaction time lasting to 10 h. Broken microspheres can be found in Fig. 2d, f, which indicates the formation of hollow structure. The cross-section morphology of the samples can be clearly observed from the area highlighted by the red dots (Fig. 2d). The surface of hollow spheres is rough and the shell thickness is approximately 150 nm.

To confirm the hollow structure, the sample was further examined by TEM. The hollow structure can be clearly observed in Fig. 3a–c. The shell thickness is about 150 nm, which is consistent with the SEM results. The high-resolution image (Fig. 3d) reveals that the $TiO_2$ hollow microsphere comprises fine nanocrystallites of approximately 10 nm, which is in good correspondence to the XRD result. The lattice spacing of 0.35 nm is associated with the (101) plane of anatase phase.

To investigate the effect of $NH_4HCO_3$ on the formation of $TiO_2$ hollow spheres, samples were prepared following the same synthesis procedure except for the replacement of 4 g $NH_4HCO_3$ by 1 and 2 g $NH_4HCO_3$ during the solvothermal process. Supplementary Fig. S1 shows the XRD results of the hollow $TiO_2$ samples prepared with 1 g (a), 2 g (b), and 4 g (c)

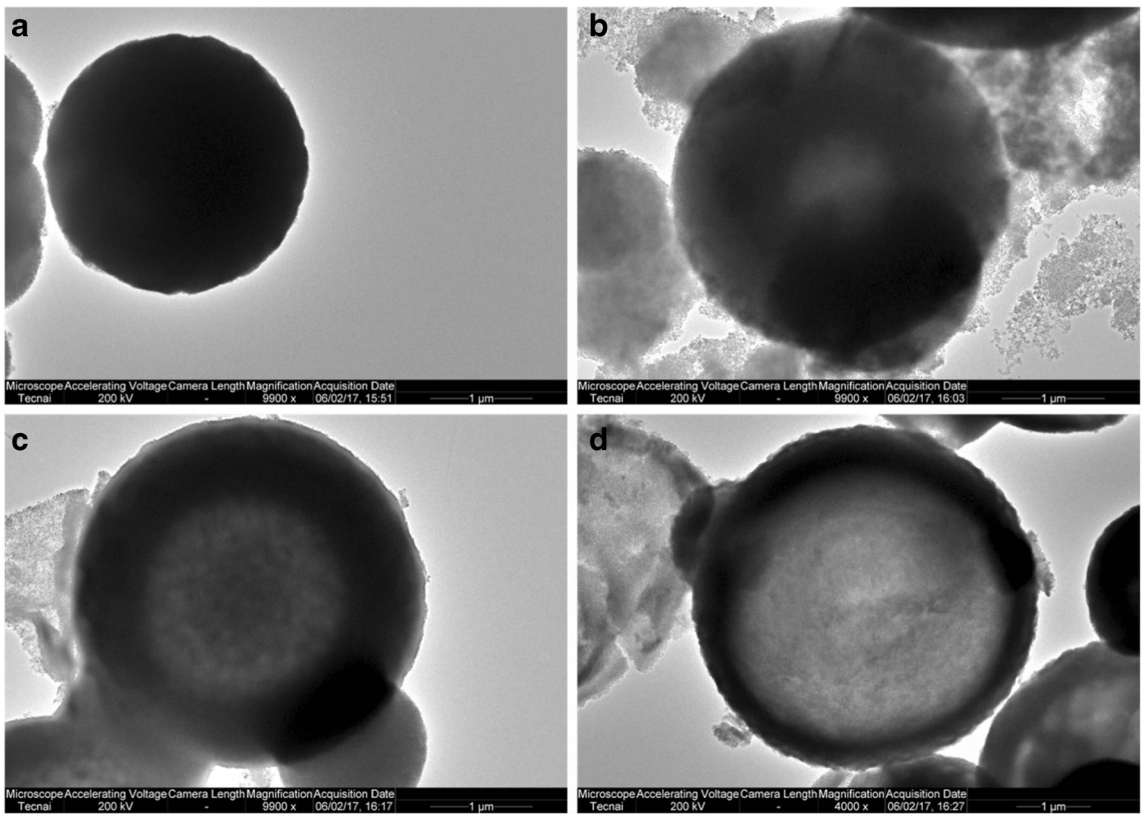


**Fig. 4** TEM images of the $TiO_2$ samples prepared for **a** 1 h, **b** 3 h, **c** 6 h, and **d** 10 h

$NH_4HCO_3$. No detectable difference can be observed, indicating that the amount of $NH_4HCO_3$ has no influence on phase structure. The typical SEM images are shown in Fig. S2. Microspheres with diameters in the range of 1.0–4.0 μm can be observed for both samples, revealing that the morphology has no variation along with the change on $NH_4HCO_3$ amount.

The role of $NH_4HCO_3$ in this work is a matter of the precursor for producing intermediate $H_2O$ through its decomposition at high temperature (Eq. (2)). Then, TBOT hydrolyses with the generated $H_2O$ to form $TiO_2$ particles, as illustrated in Eqs. (3–7) [45]. Furthermore, the formation of hollow $TiO_2$ microspheres follows a typical inside-out Ostwald ripening, as shown in Scheme 2. To demonstrate this formation mechanism of hollow $TiO_2$ microspheres, the samples prepared for different time (1 h, 3 h, 6 h, 10 h) were further examined by TEM. As shown in Fig. 4, the solid structure (Fig. 4a) turned to hollow structure (Fig. 4d) gradually with the time increasing, and thickness of the shell also became thinner and thinner. These results are consistent with the Ostwald ripening mechanism that the inside small $TiO_2$ nanoparticles gradually dissolve and transfer to microspheres surface, and outer $TiO_2$ nanoparticles trend to coarsen during the solvothermal treatment based on the Ostwald ripening. The mass transport from the center to outward, leading to the formation of hollow structure [46, 47].

$$NH_4HCO_3 \xrightarrow{\Delta} NH_3\uparrow + CO_2\uparrow + H_2O \quad (2)$$

$$Ti(OBu)_4 + H_2O \rightarrow Ti(OBu)_3(OH) + BuOH \quad (3)$$

$$Ti(OBu)_3(OH) + H_2O \rightarrow Ti(OBu)_2(OH)_2 + BuOH \quad (4)$$

$$Ti(OBu)_2(OH)_2 + H_2O \rightarrow Ti(OBu)(OH)_3 + BuOH \quad (5)$$

$$Ti(OBu)(OH)_3 + H_2O \rightarrow Ti(OH)_4 + BuOH \quad (6)$$

$$Ti(OH)_4 \rightarrow TiO_2 + 2H_2O \quad (7)$$

The nitrogen adsorption-desorption isotherms and the pore size distribution curve of the samples synthesized for 3 h (a), 6 h (b), and 10 h (c) are exhibited in Fig. 5. The isotherms of each sample can be well indexed to type IV isotherms. The specific surface area of the $TiO_2$ hollow microspheres for 3, 6, and 10 h are 158, 179, and 180 $m^2\ g^{-1}$ respectively according to the BET equation. The inset images in Fig. 5a–c show that a same narrow pore size distribution at approximately 5–10 nm

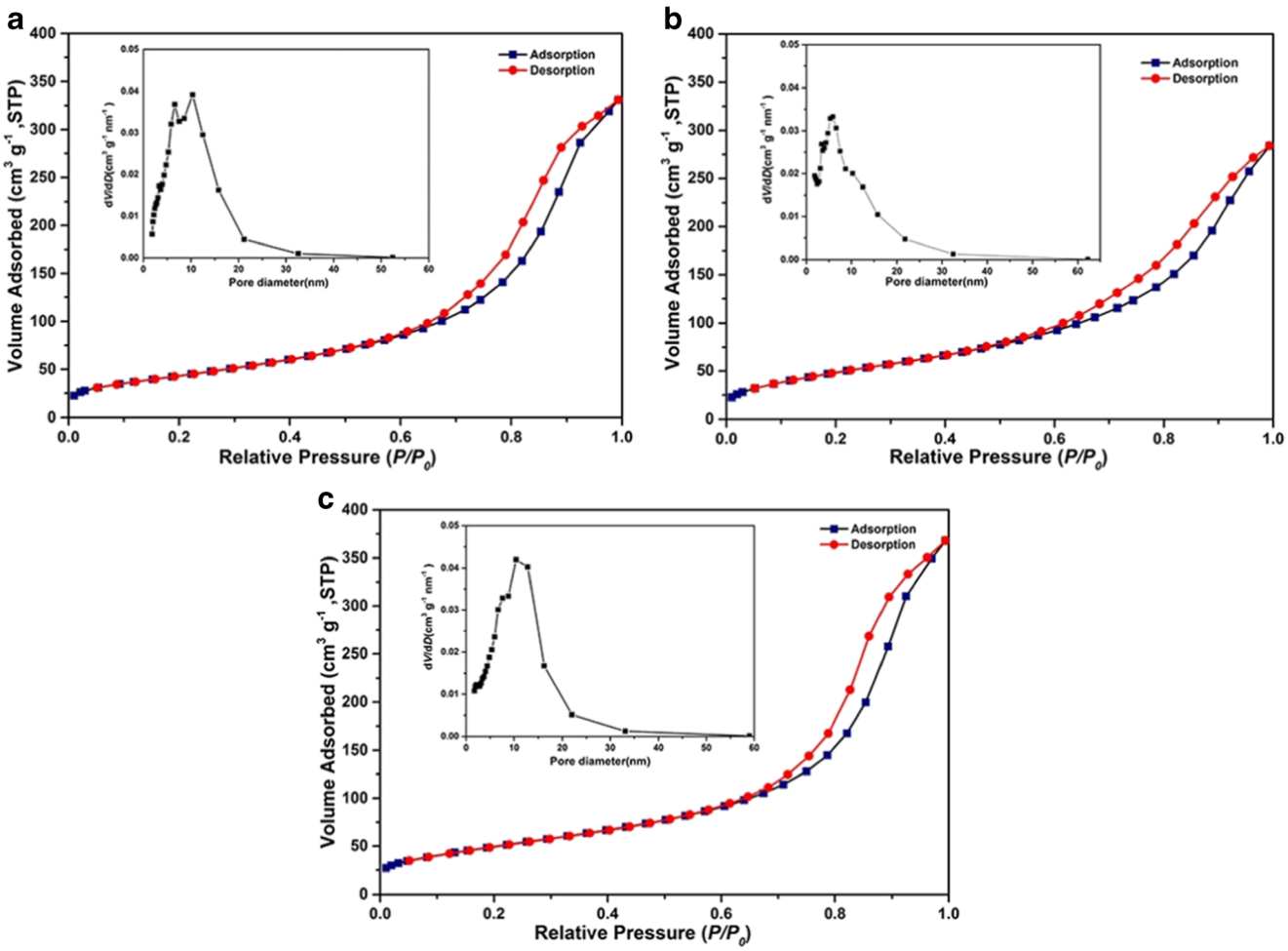


**Fig. 5** The nitrogen adsorption-desorption isotherms of the hollow $TiO_2$ samples prepared for **a** 3 h, **b** 6 h, and **c** 10 h

**Table 1** Textural properties of the hollow $TiO_2$ samples prepared for different reaction time

| No. | Reaction time (h) | Specific surface area ($m^2\ g^{-1}$) | Average pore size (nm) | Pore volume ($cm^3\ g^{-1}$) |
|---|---|---|---|---|
| 1 | 3 | 158 | 9.0 | 0.51 |
| 2 | 6 | 179 | 7.8 | 0.43 |
| 3 | 10 | 180 | 9.6 | 0.57 |
| P25 | — | 50 | — | — |

can be observed for all samples. The average pore size of the sample for 3, 6, and 10 h is 9.0, 7.8, and 9.6 nm, respectively, indicating spacing between the crystals [43]. The detailed textural properties including specific surface area, average pore size and pore volume of these three samples and the specific surface area data of P25 are summarized in Table 1. Compared to the specific surface area of P25 (50 $m^2\ g^{-1}$) [48], much larger specific surface area was observed for all samples. The specific surface area increases when the reaction time extends to 6 h, the hollow structure began to be formed during this process, but a little enlargement is detected for further lasting to 10 h, indicating the complete formation of the hollow structure.

Figure 6 shows the adsorption performance of the samples prepared under different reaction time. Figure 6a displays the adsorption spectra of a solution of MB in the presence of the samples. Obviously, the main adsorption peaks (about 664 nm) almost vanish for the sample prepared for 6 and 10 h, demonstrating the excellent adsorption performance of these two samples. As shown in Fig. 6b, it can be calculated that the equilibrium adsorption amount of P25 was 1.2 mg $g^{-1}$, and 9.5, 16.7 and 17.6 mg $g^{-1}$ for the samples prepared for 3, 6, and 10 h, respectively. The enhanced adsorption property is highly credited to the enlarged specific surface area.

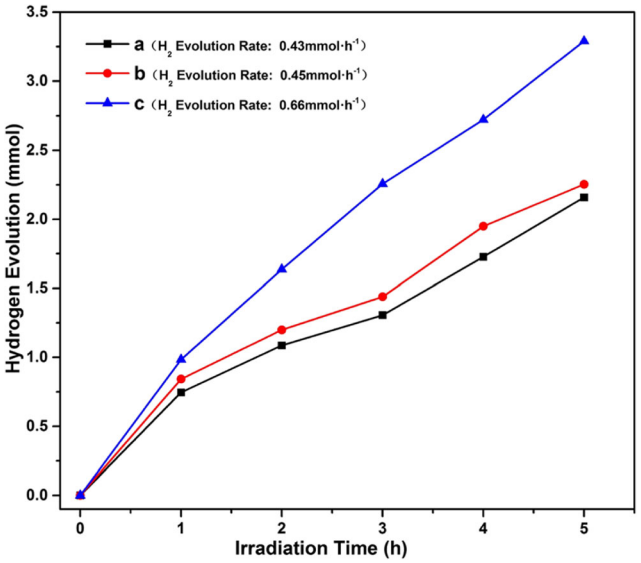


**Fig. 7** Hydrogen productions and $H_2$ evolution rates of the hollow $TiO_2$ samples prepared for 3 h (a), 6 h (b), and 10 h (c) with Pt. The reaction system was 20 mg photocatalyst in 100 mL 10% (*v*/*v*) methanol-water solution

The photocatalytic performance of the $TiO_2$ samples were evaluated by water splitting hydrogen evolution. Figure 7 displays the comparison of hydrogen productions and $H_2$ evolution rates of the samples. For the sample prepared at 250 °C for 3 h, 2.1 mmol $H_2$ has been evolved in 5 h and the $H_2$ evolution rate is 0.43 mmol $h^{-1}$. A slight increase of $H_2$ evolution was observed for the sample prepared for 6 h, the $H_2$ evolution rate is 0.45 mmol $h^{-1}$. Apparently, the sample exhibits higher $H_2$ evolution activity that 3.3 mmol $H_2$ is generated in 5 h and the $H_2$ evolution rate is about 0.66 mmol $h^{-1}$ of the sample prepared for 10 h. The enhanced photocatalytic performance of the sample is attributed to the hollow structure and Pt as the co-catalyst. Besides, Fig. S3 displays the UV-vis diffusion spectra of samples before and after loading Pt, as well as commercial P25. A slight adsorption enhancement was observed in the

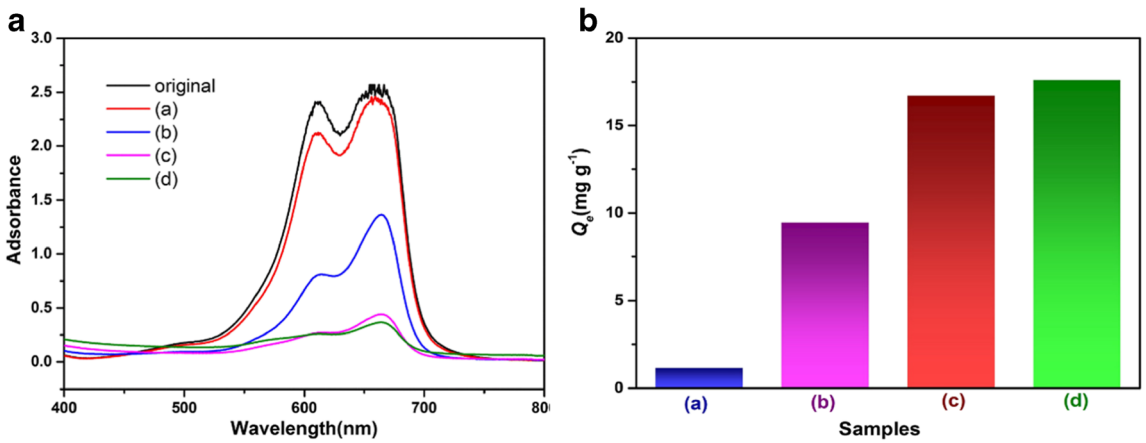


**Fig. 6** **a** Absorption spectra of a solution of MB in the presence of P25 (a) and the samples prepared for 3 h (b), 6 h (c), and 10 h (d). **b** Equilibrium adsorption amount of MB on P25 (a) and the samples prepared for 3 h (b), 6 h (c), and 10 h (d)

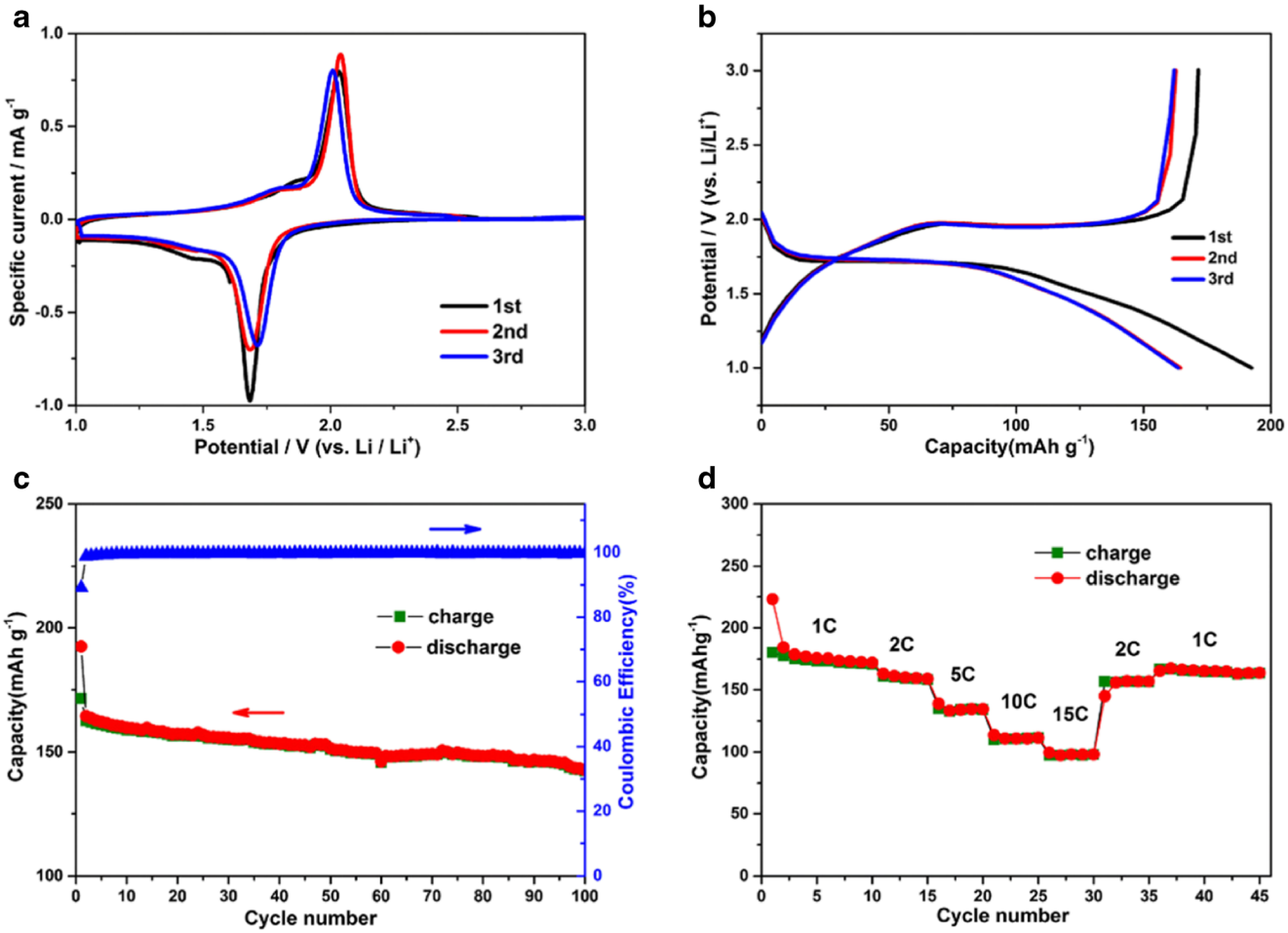


**Fig. 8** The electrochemical performance of the $TiO_2$ sample prepared for 10 h. **a** Cyclic voltammograms curves at a scan rate of 0.2 mV $s^{-1}$ within a potential window of 1.0–3.0 V (vs. $Li/Li^+$). **b** Charge-discharge voltage profiles at 300 mA $g^{-1}$. **c** Cycling performance at 300 mA $g^{-1}$. **d** Rate capability at 1 C, 2 C, 5 C, 10 C, 15 C, 2 C, and 1 C (1 C = 168 mA $g^{-1}$)

visible region of the spectra (400–800 nm). This result indicates that the hollow structure could reflect and capture more light. Much stronger adsorption covers the whole visible light region for the Pt-loaded sample, suggesting the improved visible light harvesting behavior with the presence of Pt which is consistent with our former work [49].

To further demonstrate the utility of the as-prepared $TiO_2$ hollow microspheres, the electrochemical performance as a potential anode material for LIBs was investigated. Figure 8a exhibits the CV curves for initial three cycles at a scan rate of 0.2 mV $s^{-1}$ within a potential window of 1.0–3.0 V (vs. $Li/Li^+$). In the first cycle, two well-defined peaks at 1.7 V (cathodic sweep) and 2.0 V (anodic sweep) correspond to the typical lithium insertion and extraction process, which follows the reaction mechanism illustrated in Eq. (8) [50]. And an additional weak, broad peak in Fig.8a (around 1.5 V), which only can be observed in the first cycle is ascribed to irreversible trapped lithium ions into $Li_xTiO_2$ ($x \approx 0.03$) phase [51–53]. Furthermore, the CV curves of the second and third cycles overlap well, indicating good cycling stability of the $TiO_2$ hollow microspheres.

$$TiO_2 + xLi^+ + xe^- \leftrightarrow Li_xTiO_2 \quad (8)$$

The charge–discharge voltage profiles of the first three cycles are shown in Fig. 8b for the hollow $TiO_2$ samples at a specific current of 300 mA $g^{-1}$. The voltage plateaus arise at approximately 1.7 V in the discharge curve and 2.0 V in the charge curve, respectively, which is consistent with the result of the CVs (Fig. 8a). Additionally, the discharge and charge curves of the second and third cycles are nearly overlapped, indicating a stable capacity retention of the as-prepared $TiO_2$ hollow microspheres.

Figure 8c depicts the cycling performance at a specific current of 300 mA $g^{-1}$. The discharge and charge capacities in the first cycle were 193 and 172 mAh $g^{-1}$, corresponding to a Coulombic efficiency of 89%. The irreversible capacity loss might be resulted by the formation of SEI film, $Li^+$ inserts into the irreversible site and the decomposition of electrolyte, which consume some quantity of lithium ions. Moreover, a reversible capacity remained 143 mAh $g^{-1}$ after 100 charge–discharge cycles, indicating outstanding capacity reversibility and good cycling stability of the $TiO_2$ hollow microspheres. This electrochemical

**Table 2** Comparative cycling performance of representative $TiO_2$ with hollow structure as anode for lithium-ion batteries

| Materials | Capacity/ mAh $g^{-1}$ | Specific current/mA $g^{-1}$ | Cycle number | Method | Ref. |
|---|---|---|---|---|---|
| Hollow $TiO_2$ nanospheres | 131 | 85 | 30 | Gas template | [17] |
| Yolk-shell $TiO_2$ microspheres | 133 | 336 | 40 | Template-free | [18] |
| $TiO_2$ hollow ellipsoid | 122 | 34 | 30 | Hard template | [35] |
| $TiO_2$ hollow capsule | 120 | 34 | 30 | Hard template | [35] |
| $TiO_2$ hollow pseudocube | 117 | 34 | 30 | Hard template | [35] |
| $TiO_2$ hollow peanuts | 121 | 34 | 30 | Hard template | [35] |
| $TiO_2$ hollow spheres | 142 | 60 | 40 | Hard template | [38] |
| $TiO_2$ hollow spheres | 148 | 173 | 300 | Hard template | [39] |
| Hollow $TiO_2$ spheres | 113 | 1 C | 200 | Template-free | [41] |
| $TiO_2$ hollow microspheres | 135 | 335 | 40 | Template-free | [43] |
| $TiO_2$ hollow microspheres | 143 | 300 | 100 | Template-free | This work |

performance is comparable to the results reported in the literatures [17, 18, 35, 38, 39, 41, 43], as summarized in Table 2.

The rate capability of the sample at various charge–discharge rates was measured as well. As shown in Fig. 8d, the average discharge capacities decreased to 176, 160, 134, 110, and 98 mAh $g^{-1}$ with the rates increasing to 1 C, 2 C, 5 C, 10 C and 15 C (Here 1 C is equivalent to 168 mA $g^{-1}$). When the current rate was reverted to 2 C, the capacity recovered to 157 mAh $g^{-1}$, with only 2% capacity fading. Furthermore, when the current rate decreased to 1 C, a capacity of 165 mAh $g^{-1}$ was delivered with a capacity retention ratio of 94%. As an example for detail, Han's group [41] synthesized $TiO_2$ hollow microspheres through a two-step hydrothermal process. The resultant sample exhibited specific capacities of 145, 111, 77, and 50 mAh $g^{-1}$ at 1 C, 2 C, 5 C and 10 C, respectively.

In order to investigate the potential reasons for the excellent cycling performance and rate capability of hollow $TiO_2$ microspheres, electrochemical impedance spectra (EIS) were implemented on the hollow $TiO_2$ microspheres (a) and solid $TiO_2$ microspheres (b) as shown in Fig. 9. A semicircle at high-medium frequency region is attributed to the charge transfer reaction, while an inclined line in low frequency region is correlated with the diffusion of lithium ions in the solid electrode. In the inserted equivalent circuit, $R_{ct}$ denotes the charge transfer resistance between electrolyte and electrode. The corresponding fitting data of circuit elements are listed in Table 3. As shown in Table 3, the $R_{ct}$ is 36.8 Ω for hollow $TiO_2$ microspheres, while it is 50.6 Ω for solid $TiO_2$ microspheres. The decreased $R_{ct}$ implies that better charge carrier transport than that of solid $TiO_2$ owing to the presence of the hollow structure, which can reduce the interface resistance [30, 41].

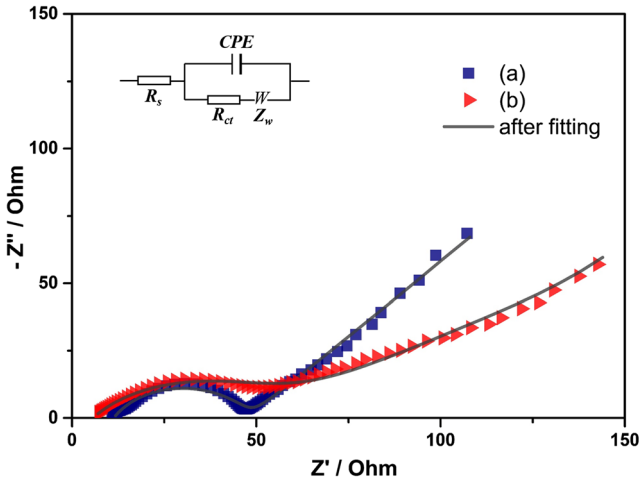


**Fig. 9** Nyquist plots of (a) the hollow $TiO_2$ microspheres (prepared for 10 h) and (b) the solid $TiO_2$ microspheres (prepared for 3 h) after 30 discharge-charge cycles and the fitting line of experimental impedance spectra using the equivalent circuit modelling as inset

Moreover, the diffusion coefficient of lithium ions for the electrodes are evaluated based on the impedance spectra using Eqs. (9, 10). In the low frequency region of Nyquist plots, Z′ is proportional to $\omega^{-1/2}$ (angular frequency), and $\sigma_w$ is the Warburg factor, which can be calculated according to Eq. (9). As shown in Table 3, the $\sigma_w$ of hollow and solid $TiO_2$ microspheres is linear fitted to be 17.8 and 43.2 Ω $s^{-1/2}$, respectively. The $Li^+$ diffusion coefficient (D) can be estimated by using Eq. (10) [51].

$$Z^{`} = R_s + R_{ct} + \sigma_W \omega^{-1/2} \tag{9}$$

$$D = \frac{R^2 T^2}{2A^2 F^4 \sigma_W^2 C^2} \tag{10}$$

**Table 3** The fitting data of the equivalent circuit elements

| | $R_s$/Ω | $R_{ct}$/Ω | $\sigma_w$ (Ω $s^{-1/2}$) | $D$ ($cm^2$ $s^{-1}$) |
|---|---|---|---|---|
| Hollow $TiO_2$ microspheres | 11.4 | 36.8 | 17.8 | $2.7 \times 10^{-12}$ |
| Solid $TiO_2$ microspheres | 5.7 | 50.6 | 43.2 | $4.5 \times 10^{-13}$ |

In Eq. (10), $R$ is the gas constant (8.3145 J $mol^{-1}$ $K^{-1}$), $T$ is 298.15 K, $A$ is the surface area of electrode, $F$ is Faraday's constant (96,485 C $mol^{-1}$) and $C$ is the molar concentration of lithium ions. The diffusion coefficient of lithium ions is $2.7 \times 10^{-12}$ $cm^2$ $s^{-1}$ of hollow $TiO_2$ microspheres, which is six times higher than that of the solid $TiO_2$ microspheres ($4.5 \times 10^{-13}$ $cm^2$ $s^{-1}$). This improvement is mainly resulted from the shorter transfer pathway due to the hollow structure with larger specific surface area and thinner shell as well.

Considering the advantages of the facile one-step strategy to synthesize $TiO_2$ hollow microspheres as well as their superior photocatalytic and excellent electrochemical performance, it should be meaningful for this work to facilitate the preparation and application of anatase $TiO_2$.

## Conclusions

In summary, we have developed a one-step template-free approach to fabricate $TiO_2$ hollow microspheres through a modified solvothermal method with the assistance of $NH_4HCO_3$. As a kind of photocatalyst, the hollow $TiO_2$ microspheres exhibit a high hydrogen evolution ability. The $H_2$ evolution rate of the optimal sample is about 0.66 mmol $h^{-1}$ after loaded with 1 wt.% Pt. As an anode material for LIBs, the initial discharge capacity was 193 mAh $g^{-1}$ and remained at 143 mAh $g^{-1}$ at 300 mA $g^{-1}$ after 100 cycles. Furthermore, the specific capacity was maintained at 98 mAh $g^{-1}$, even at the high rate of 15 C. The impressive photocatalytic performance and lithium storage capabilities can be attributed to the hollow structure of the sample. Considering the features of low cost and simple preparation, the proposed template-free method may transfer to synthesize other relevant oxide materials.

**Acknowledgements** This work was partially supported by the National Natural Science Foundation of China (No. 21273047) and Key Laboratory of Functional Inorganic Material Chemistry (Heilongjiang University), Ministry of Education. We really appreciate the referees' valuable comments, which have greatly improved the quality of the manuscript.

## References

1. Ma Y, Wang X, Jia Y, Chen X, Han H, Li C (2014) Titanium dioxide-based nanomaterials for photocatalytic fuel generations. Chem Rev 114:9987–10043
2. Kapilashrami M, Zhang Y, Liu YS, Hagfeldt A, Guo J (2014) Probing the optical property and electronic structure of $TiO_2$ nanomaterials for renewable energy applications. Chem Rev 114: 9662–9707
3. Songa T, Paik U (2016) $TiO_2$ as an active or supplemental material for lithium batteries. J Mater Chem A 4:14–31
4. Yan X, Wang Z, He M, Hou Z, Xia T, Liu G, Chen X (2015) $TiO_2$ nanomaterials as anode materials for lithium-ion rechargeable batteries. Energ Technol 3:801–814
5. Bai Y, Mora-Seró I, Angelis FD, Bisquert J, Wang P (2014) Titanium dioxide nanomaterials for photovoltaic applications. Chem Rev 114:10095–10130
6. Chen X, Shen S, Guo L, Mao SS (2010) Semiconductor-based photocatalytic hydrogen generation. Chem Rev 110:6503–6570
7. Zhou X, Häublein V, Liu N, Nguyen NT, Zolnhofer EM, Tsuchiya H, Killian MS, Meyer K, Frey L, Schmuki P (2016) $TiO_2$ nanotubes: nitrogen-ion implantation at low dose provides noble-metal-free photocatalytic $H_2$-evolution activity. Angew Chem Int Ed 55: 3763–3767
8. Sun S, Gao P, Yang Y, Yang P, Chen Y, Wang Y (2016) N-doped $TiO_2$ nanobelts with coexposed (001) and (101) facets and their highly efficient visible-light-driven photocatalytic hydrogen production. ACS Appl Mater Interfaces 8:18126–18131
9. Meng A, Zhang J, Xu D, Cheng B, Yu J (2016) Enhanced photocatalytic $H_2$-production activity of anatase $TiO_2$ nanosheet by selectively depositing dual-cocatalysts on {101} and {001} facets. Appl Catal B Environ 198:286–294
10. Wang Y, Cai J, Wu M, Zhang H, Meng M, Tian Y, Ding T, Gong J, Jiang Z, Li X (2016) Hydrogenated cagelike titania hollow spherical photocatalysts for hydrogen evolution under simulated solar light irradiation. ACS Appl Mater Interfaces 8:23006–23014
11. Cai J, Wu X, Li S, Zheng F (2017) Controllable location of au nanoparticles as cocatalyst onto $TiO_2$@$CeO_2$ nanocomposite hollow spheres for enhancing photocatalytic activity. Appl Catal B Environ 201:12–21
12. Zhou Y, Yoon S (2014) Interconnected carbon-decorated $TiO_2$ nanocrystals with enhanced lithium storage performance. Electrochem Commun 40:54–57
13. Geng H, Cao X, Zhang Y, Geng K, Qu G, Tang M, Zheng J, Yang Y, Gu H (2015) Hollow nanospheres composed of titanium dioxide nanocrystals modified with carbon and gold for high performance lithium ion batteries. J Power Sources 294:465–472
14. Singh DP, Mulder FM, Wagemaker M (2013) Templated spinel $Li_4Ti_5O_{12}$ Li-ion battery electrodes combining high rates with high energy density. Electrochem Commun 35:124–127
15. Liu L, Fan Q, Sun C, Gu X, Li H, Gao F, Chen Y, Dong L (2013) Synthesis of sandwich-like $TiO_2$@C composite hollow spheres with high rate capability and stability for lithium-ion batteries. J Power Sources 221:141–148
16. Cong DP, Kim JH, Jeong SY, Choi JH, Kim J, Cho CR (2015) Enhanced electrochemical performance of carbon-coated $TiO_2$ nanobarbed fibers as anode material for lithium-ion batteries. Electrochem Commun 60:204–207
17. Long L, Zhang H, Ye M, Fang Z (2015) Ammonia cation-assisted bubble template for synthesizing hollow $TiO_2$ nanospheres and their application in lithium ion storage. RSC Adv 5:12224–12229
18. Wang X, Wang Y, Yang L, Wang K, Lou X, Cai B (2014) Template-free synthesis of homogeneous yolk-shell $TiO_2$ hierarchical microspheres for high performance lithium ion batteries. J Power Sources 262:72–78
19. Qiao H, Xiao L, Zhang L (2008) Phosphatization: a promising approach to enhance the performance of mesoporous $TiO_2$ anode for lithium ion batteries. Electrochem Commun 10:616–620
20. Xiu Z, Alfaruqi MH, Gim J, Song J, Kim S, Duong PT, Baboo JP, Mathew V, Kim J (2016) MOF-derived mesoporous anatase $TiO_2$ as anode material for lithium-ion batteries with high rate capability and long cycle stability. J Alloys Compd 674:174–178
21. Larcher D, Tarascon JM (2015) Towards greener and more sustainable batteries for electrical energy storage. Nat Chem 7:19–29
22. Li H, Wang Z, Chen L, Huang X (2009) Research on advanced materials for Li-ion batteries. Adv Mater 21:4593–4607
23. Roy P, Srivastava SK (2015) Nanostructured anode materials for lithium ion batteries. J Mater Chem A 3:2454–2484
24. Liu L, Peng J, Wang H, Ma Y, Yu F, Dai B, Guo XH, Wong CP (2016) Synthesis of mesoporous $TiO_2$@C@$MnO_2$ multi-shelled

hollow nanospheres with high rate capability and stability for lithium-ion batteries. RSC Adv 6:65243–65251
25. Peng L, Zhang H, Bai Y, Feng Y, Wang Y (2015) A designed $TiO_2$/carbon nanocomposite as a high-efficiency lithium-ion battery anode and photocatalyst. Chem Eur J 21:14871–14878
26. Yue W, Randorn C, Attidekou PS, Su Z, Irvine JTS, Zhou W (2009) Syntheses, Li insertion, and photoactivity of mesoporous crystalline $TiO_2$. Adv Funct Mater 19:2826–2833
27. Xia T, Zhang W, Murowchick JB, Liu G, Chen X (2013) A facile method to improve the photocatalytic and lithium-ion rechargeable battery performance of $TiO_2$ nanocrystals. Adv Energy Mater 3: 1516–1523
28. Khan J, Gu J, Meng Y, Chai Z, He S, Wu Q, Tong S, Ahmed G, Mai W, Wu M (2017) Anatase $TiO_2$ single crystal hollow nanoparticles: their facile synthesis and high-performance in dye-sensitized solar cells. CrystEngComm 19:325–334
29. Zhang J, Li L, Xiao Z, Liu D, Wang S, Zhang J, Hao Y, Zhang W (2016) Hollow sphere $TiO_2$−$ZrO_2$ prepared by self-assembly with polystyrene colloidal template for both photocatalytic degradation and $H_2$ evolution from water splitting. ACS Sustain Chem Eng 4: 2037–2046
30. Ren H, Yu R, Wang J, Jin Q, Yang M, Mao D, Kisailus D, Zhao H, Wang D (2014) Multishelled $TiO_2$ hollow microspheres as anodes with superior reversible capacity for lithium ion batteries. Nano Lett 14:6679–6684
31. Grabowskaa E, Marcheleka M, Klimczukb T, Trykowskic G, Zaleska-Medynska A (2016) A noble metal modified TiO2 microspheres: surface properties and photocatalytic activity under UV–vis and visible light. J Mol Catal A Chem 423:191–206
32. Wang C, Liu H, Liu Y, He G, Jiang C (2014) Comparative activity of $TiO_2$ microspheres and P25 powder for organic degradation: implicative importance of structural defects and organic adsorption. Appl Surf Sci 319:2–7
33. Prieto G, Tüysüz H, Duyckaerts N, Knossalla J, Wang GH, Schüth F (2016) Hollow nano- and microstructures as catalysts. Chem Rev 116:14056–14119
34. Zhu F, Wu D, Li Q, Dong H, Li J, Jiang KXD (2012) Hierarchical $TiO_2$ microspheres: synthesis, structural control and their applications in dye-sensitized solar cells. RSC Adv 2:11629–11637
35. Wang Y, Su X, Lu S (2012) Shape-controlled synthesis of $TiO_2$ hollow structures and their application in lithium batteries. J Mater Chem 22:1969–1976
36. Yang LP, Lin XJ, Zhang X, Zhang W, Cao AM, Wan LJ (2016) General synthetic strategy for hollow hybrid microspheres through a progressive inward crystallization process. J Am Chem Soc 138: 5916–5922
37. Liu H, Li W, Shen D, Zhao D, Wang G (2015) Graphitic carbon conformal coating of mesoporous $TiO_2$ hollow spheres for high-performance lithium ion battery anodes. J Am Chem Soc 137: 13161–13166
38. Wang J, Bai Y, Wu M, Yin J, Zhang WF (2009) Preparation and electrochemical properties of $TiO_2$ hollow spheres as an anode material for lithium-ion batteries. J Power Sources 191:614–618
39. Zhang G, Wu HB, Song T, Paik U, Lou XW (2014) $TiO_2$ hollow spheres composed of highly crystalline nanocrystals exhibit superior lithium storage properties. Angew Chem Int Ed 126: 12798–12801
40. Zhong Z, Yin Y, Gates B, Xia Y (2000) Preparation of mesoscale hollow spheres of $TiO_2$ and $SnO_2$ by templating against crystalline arrays of polystyrene beads. Adv Mater 12:206–209
41. Han C, Yang D, Yang Y, Jiang B, He Y, Wang M, Song AY, He YB, Li B, Lin Z (2015) Hollow titanium dioxide spheres as anode material for lithium ion battery with largely improved rate stability and cycle performance by suppressing the formation of solid electrolyte interface layer. J Mater Chem A 3:13340–13349
42. Jiang F, Zheng SR, An LC, Chen H (2012) Effect of calcination temperature on the adsorption and photocatalytic activity of hydrothermally synthesized $TiO_2$ nanotubes. Appl Surf Sci 258:7188–7194
43. Wang X, Meng Q, Wang Y, Liang H, Bai Z, Wang K, Lou X, Cai B, Yang L (2016) $TiO_2$ hierarchical hollow microspheres with different size for application as anodes in high-performance lithium storage. Appl Energy 175:488–494
44. Chen JS, Lou XW (2009) Anatase $TiO_2$ nanosheet: an ideal host structure for fast and efficient lithium insertion/extraction. Electrochem Commun 11:2332−2335
45. Zhang X, Sun Y, Cui X, Jiang Z (2012) Carbon-incorporated $TiO_2$ microspheres: facile flame assisted hydrolysis of tetrabutyl orthotitanate and photocatalytic hydrogen production. Int J Hydrogen Energy 37:1356−1365
46. Rui Y, Wang L, Zhao J, Wang H, Li Y, Zhang Q, Xu J (2016) Template-free synthesis of hierarchical $TiO_2$ hollow microspheres as scattering layer for dye-sensitized solar cells. Appl Surf Sci 369: 170–177
47. Si L, Huang Z, Lv K, Ye H, Deng K, Wu Y (2014) Fabrication of $TiO_2$ hollow microspheres by ammonia-induced self-transformation. J Alloy Compd 612:69−73
48. Kirchnerova J, Cohen MLH, Guy C, Klvana D (2005) Photocatalytic oxidation of n-butanol under fluorescent visible light lamp over commercial $TiO_2$ (Hombicat UV100 and Degussa P25). Appl Catal A-Gen 282:321–332
49. Li H, Zhang XY, Cui XL (2014) A facile and waste-free strategy to fabricate Pt-C/$TiO_2$ microspheres: Enhanced photocatalytic performance for hydrogen evolution. Int J Photoenergy 2014:1−9
50. Jin J, Huang SZ, Shu J, Wang HE, Li Y, Yu Y, Chen LH, Wang BJ, Su BL (2015) Highly porous $TiO_2$ hollow microspheres constructed by radially oriented nanorods chains for high capacity, high rate and long cycle capability lithium battery. Nano Energy 16:339−349
51. Chen Y, Li ZF, Shi S, Song CY, Jiang ZY, Cui XL (2017) Scalable synthesis of $TiO_2$ crystallites embedded in bread-derived carbon matrix with enhanced lithium storage performance. J Mater Sci: Mater Electron 28:9206−922
52. Zhao CY, Liu LJ, Zhang QY, Rogers J, Zhao HL, Li Y (2015) Synthesis of carbon-$TiO_2$ nanocomposites with enhanced reversible capacity and cyclic performance as anodes for lithium-ion batteries. Electrochim Acta 155:288–296
53. Li MS, Li XF, Li WH, Meng XB, Yu Y, Sun XL (2015) Atomic layer deposition derived amorphous $TiO_2$ thin film decorating graphene nanosheets with superior rate capability. Electrochem Commun 57:43–47